Submitted to IEEE Transactions on Pattern Analysis and Machine Intelligence (PAMI)

Positron Emission Tomography (PET) Image Reconstruction: Revisited. Part-I

Partha P. Mondal K.Rajan[1] and Sitharama Iyengar [2]

Abstract

This paper attempts to construct a goal seeking approach for modeling a system that requires correction to reduce uncertainties by using additional context information and constraints such as positivity of density estimates and optimal smoothing. The additional information becomes available to the system as the iteration progresses. Based on the prior knowledge, a decision is taken for the output to be in the desired tolerance limits. In this work, positron emission tomography (PET) image reconstruction system is projected as a good example of goal seeking paradigm. The image reconstructed using the proposed algorithm was found to have a percent error of 23.77% after 50 iterations. The ML, MAP and MRP algorithms, for the same number of iterations, have produced images with 32.61%, 24.95% and 24.54% respectively. The experimental results are very encouraging and interesting.

1. Introduction

Medical imaging modalities like PET and SPECT demand high quality artifact-free images, which become the basis for studying physiological and neurological processes. Recent studies have shown that PET is sensitive to biological processes like metabolism and diseases [1]. PET modality is found to be more sensitive in detecting biological abnormalities, which are found to produce no changes in X-ray computed tomography (CT) and magnetic resonance imaging (MRI). Model-based iterative approaches to PET image reconstruction allow optimal noise handling and accurate system response modeling. Research in PET is focused on three key issues :

(1) How to select a potential function (embedded in cost function) with desired image properties.

(2) How to produce images faster to enable real time realization.

[1]Partha P Mondal and K Rajan are with department of Physics, Indian Institute of Science, Bangalore, INDIA.
[2]Sitharama Iyengar is with Department of Computer Science, Louisiana State University, Baton Rouge, LA. E-mail: iyengar@bit.csc.lsu.edu
This work was supported by Council of Scientific and Industrial Research, New Delhi, INDIA.

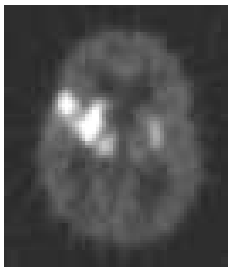

Figure 1: Real PET image of a brain slice.

(3) How to improve the quality of the reconstructed images.

In this work, we have focused on issue (1). With the rapid development of high speed processors like digital signal processor and media processor, it is possible to address the second issue to a satisfactory limit [4][5]. Further, various algorithmic methods have been suggested for accelerating the convergence of the maximum likelihood (ML) algorithm [6-12, 23].

PET image reconstruction is a complex process due to the large number of variables involved. Hence, a systematic approach needs to be developed for a stable and desired output (image). Towards this, a goal seeking paradigm is developed for PET which supports uncertainty management [18]. Uncertainty is naturally embedded in PET image reconstruction, first due to incomplete data, and second, due to the noise embedded in the measurement data. Measurement data is incomplete due to a finite number of detectors. Data space is connected to image space by an maximum likelihood / maximum $a-posteriori$ (ML/MAP) operator and hence, the shadow of noise in data space is reflected in the image space as well. The image space is connected to the data space by a many-to-one mapping, in which each pixel is a sensor. Image sensor is related to all the data sensors (tube detectors) that pass through it. Though, the measurement data is uncorrelated (independent Poisson process), the corresponding image sensors (pixels) are highly correlated. It is this correlation that is being taken advantage of, to enhance the image quality. A strong correlation between the image sensors (image pixels) is believed to exist [13-17]. Goal seeking paradigm is found suitable for this type of modeling [18]. This is a very generalized way of visualizing the MAP problem [13-17]. Fig. 1 shows an example of a real PET image, where the localization of the metabolic activity during epilepsia treatment is very clearly visible.

The organization of the paper is as follows. Section 2 provides a brief description of ML and MAP image reconstruction approaches used in PET. In Section 3, PET image reconstruction problem is projected in a goal seeking paradigm [18] and a rule based approach towards PET image reconstruction problem is proposed. The proposed algorithm is summarized in section 4. Section 5 describes the implementation issues and the evaluation of the proposed algorithm, followed by conclusions in Section 6.

2. General Description of PET Image Reconstruction

The measurements in PET, y_j , j=1,...,M are modeled as independent Poisson random variables with mean parameters, $\zeta_j = \sum_{i=1}^{N}(\lambda_i\ p_{ij})$, j=1,...,M , where λ_i , i=1,...,N are the mean parameters of the emission process and p_{ij} is the probability that an annihilation in the i^{th} pixel is detected in j^{th} detector. The likelihood function (which is the joint probability of an annihilation event anywhere in the object (image domain) and getting counted in the detector system) is given by,

$$P(y/\lambda) = \prod_{j=1}^{M} Poisson(y_j;\ \sum_{i=1}^{N} \lambda_i\ p_{ij}). \tag{1}$$

Maximum Likelihood (ML) reconstruction can be formulated as,

$$\lambda^{ML} = \max_{\lambda>0}[\ logP(y/\lambda)\ ]. \tag{2}$$

An iterative equation using ML-algorithm for obtaining the density estimates $\lambda_i;\ i = 1, ..., N$ is given by [3],

$$\lambda_i^{k+1} = \frac{\lambda_i^k}{\sum_{j=1}^{M} p_{ij}} \sum_{j=1}^{M} \frac{y_j p_{ij}}{\sum_{i=1}^{N} \lambda_i^k p_{ij}}. \tag{3}$$

It is found that, due to dimensional instability problem which is fundamental to the application of unconstrained ML estimation of density function based on point process data, reconstructed image becomes noisier with increasing iterations [26]. To solve the noise problem, another class of algorithms called maximum a-posterior (MAP) approaches were formulated [13-17]. In MAP approach, the image field is assumed to be a Markov random field (MRF) [16] and by Hammerseley-

Clifford theorem [23], image λ is characterized by Gibbs distribution,

$$P(\lambda) = \frac{1}{Z}\exp\left\{-\frac{1}{\beta}\sum_{i}\sum_{j\epsilon N_i} w_{ij}V(\lambda_i,\lambda_j)\right\} \tag{4}$$

where, Z is the normalizing constant for the distribution, β is the Gibbs hyper-parameter, w_{ij} is the weight connecting the pixel i with the neighboring pixels $j\epsilon N_i$ [15], N_i is the nearest neighbor set of pixel i and $V(\lambda_i,\lambda_j)$ is termed as the potential at site i due to the nearest neighbor elements j.

MAP algorithm determines that estimate λ^{MAP} as the solution which maximizes the posterior density function $P(\lambda/y)$ or equivalently the log of $P(\lambda/y)$. Given a suitable prior $P(\lambda)$, MAP-reconstruction can be formulated as,

$$\lambda^{MAP} = \max_{\lambda>0}[\ logP(y/\lambda) + logP(\lambda)\ ] \tag{5}$$

Solution for eqn.(4) is very difficult due to the complicated nature of the prior. Green [15] has proposed one step late (OSL) approximation for an iterative update to the MAP-problem and is given by,

$$\lambda_i^{k+1} = \frac{\lambda_i^k}{\left[\sum_{j=1}^{M} p_{ij} + \frac{1}{\beta}\sum_{j\epsilon N_i} w_{ij}\left(\frac{\partial V(\lambda_i,\lambda_j)}{\partial\lambda_i}\right)_{\lambda_i=\lambda_i^k}\right]}\sum_{j=1}^{M}\frac{y_j p_{ij}}{\sum_{i=1}^{N}\lambda_i^k p_{ij}}. \tag{6}$$

Given the iterative OSL-algorithm (eqn.(6)), the next step is the proper modeling of the potential function $V(\lambda_i,\lambda_j)$.

The general description of ML and MAP in a goal seeking paradigm [18] is schematically shown in Fig.2.

3. Proposed Rule Based Potential Function in goal seeking Paradigm

In this section of the paper, we propose a rule based PET image reconstruction in a goal seeking paradigm [18]. Each pixel is considered as a sensor in the image domain. A pixel is influenced by neighboring pixels. In this model, the weight is scaled based on the spatial distance between these pixels. Now the task for each image sensor (pixel) i is to update its value based on its

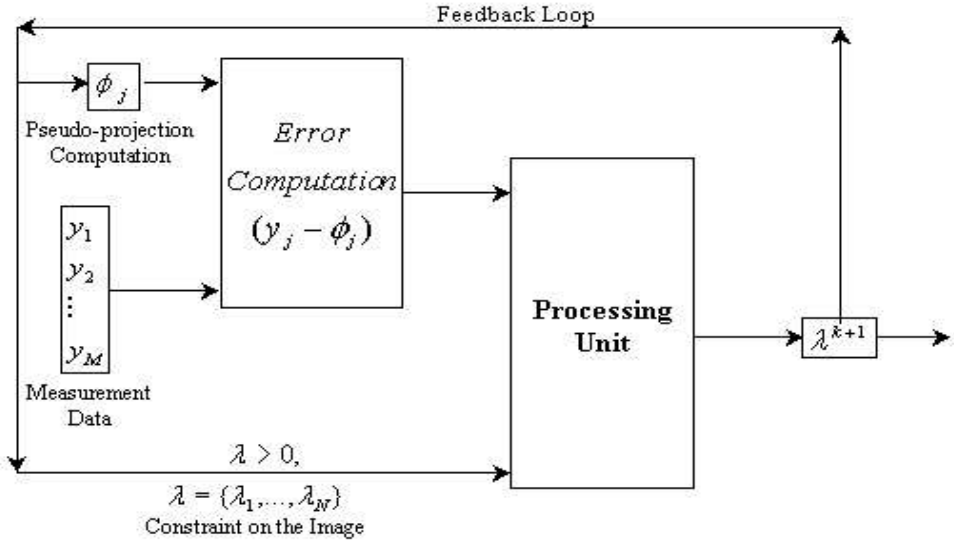

(a)

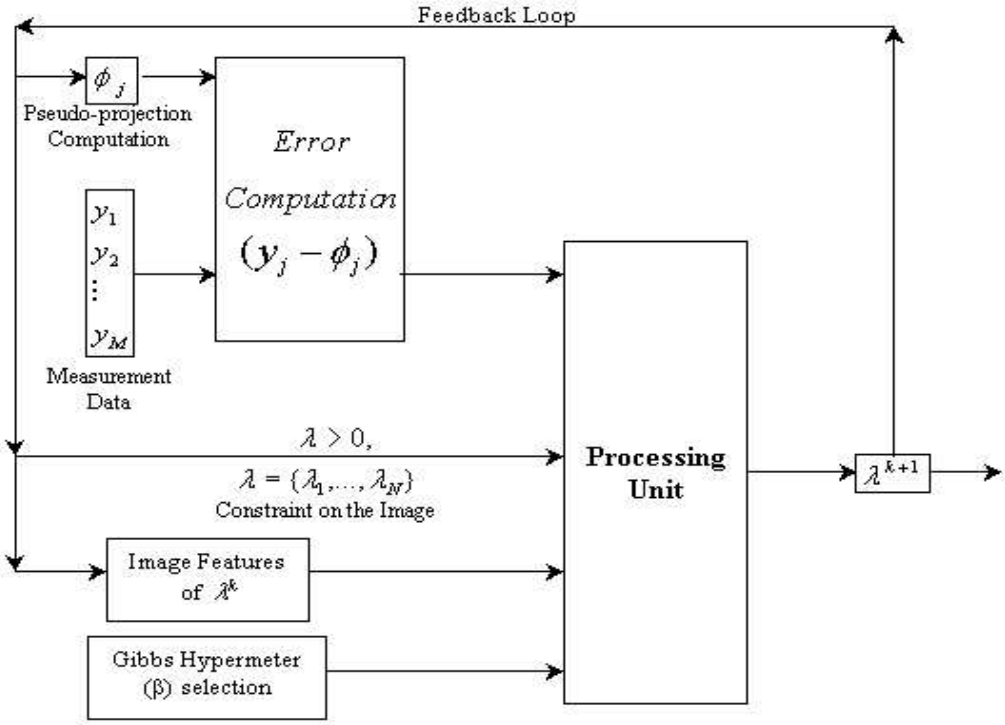

(b)

Figure 2: (a) ML and (b) MAP algorithms viewed as a goal seeking paradigm.

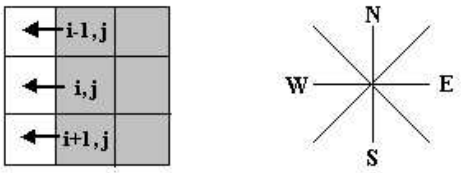

Figure 3: 3×3 neighborhood of a central pixel (i,j), showing the directional derivative along $\hat{W}$.

current value and the value of the neighborhood sensor's (pixels) value j. For such a formalism, Bayesian rule is used to connect the prior function, likelihood function and the posterior function. Since the measurement data are from a random Poisson process (Radio-nuclei emission), they are independent and uncorrelated. On the other hand, in the image domain, the neighboring pixels (sensors) are highly correlated and hence, uncertainty in the image sensor (pixel) value can be minimized by taking into account the contribution from neighboring sensors (pixel). Correlation is invoked in the reconstruction process by defining the prior function on the image domain, while the contribution from uncorrelated part (measurement data) is obtained through the likelihood function. So, MAP formulation benefits from both the uncorrelated (measurement data) as well as the correlated part (prior function). Additionally, the image constraint block in Fig.2 makes sure that the iteration process survives (due to the multiplicative nature of ML). The Bayes rule is given by,

$$P(\lambda/y) = \frac{P(y/\lambda)\ P(\lambda)}{P(y)}. \tag{7}$$

The MAP formulation is given by,

$$\lambda^{MAP} = \max_{\lambda>0}[logP(\lambda/y)]$$

$$= \max_{\lambda>0}[\ logP(y/\lambda) + logP(\lambda)\ ]. \tag{8}$$

where, likelihood function $logP(y/\lambda)$ and prior function $P(\lambda)$ are given by eqn(1) and eqn(4) respectively.

In the proposed scheme, a rule based potential function is adopted. Local derivatives are used to identify the presence of edges in the neighborhood of a pixel i, along all the directions. For

example (Fig. 3), for a 3×3 neighborhood, an edge is assumed to be absent along the north-south direction iff 2 out of 3 local derivatives $(\nabla(i,j), \nabla(i-1,j), \nabla(i+1,j))$ are small and hence, the corresponding decisive derivative $\nabla_F^k(i,j)$ is small. The derivative $\nabla^k(i,j)$ for the pixel centered at (i,j), along the direction $\hat{D}$ at k^{th} iteration is $\nabla^k(i,j)\ \hat{D} \ = \ \mid \lambda^k(i,j) - \lambda^k(*,*) \mid \hat{D}$, where, $\lambda^k(*,*)\hat{D}$ represents the nearest pixel value along the unit directional vector $\hat{D}$. We have considered 8 directions (viz. $\hat{E}, \hat{W}, \hat{N}, \hat{S}, \hat{NE}, \hat{NW}, \hat{SE}, \hat{SW}$) as shown in Fig.3. A reasonable threshold for distinguishing between the two possibilities (small or large) is $b = \frac{1}{8} \sum_{\hat{D}} \nabla(i,j)\hat{D}$. The purpose for the rule based formulation is to approximately separate the intensity variation due to the image structure and due to noise.

The following rules are formulated for quantizing the correction to a pixel (i,j):

$$\begin{aligned} &\text{if } \nabla_F^k(i,j)\hat{D} \text{ is } \textbf{small}, \\ &\quad then\ \Delta^k(i,j)\hat{D} = \nabla^k(i,j)\hat{D} \\ &\quad else,\ \Delta^k(i,j)\hat{D} = 0 \end{aligned} \tag{9}$$

where, $\Delta^k(i,j)\hat{D}$ is the correction for the pixel (i,j) from the direction $\hat{D}$. Eight such contributions are collected from all the eight directions. The total correction term $\Delta_T^k(i,j)$ for pixel at (i,j) is given by,

$$\Delta_T^k(i,j) = \frac{1}{8} \sum_{\hat{D}} \Delta^k(i,j)\hat{D} \tag{10}$$

It should be noted that, the image feature block shown in Fig. 2 is in essence, the correction term $\Delta_T^k(i,j)$.

Replacing the error term $\frac{1}{\beta} \sum_{j \epsilon N_i} \left(\frac{\partial V(\lambda_i, \lambda_j)}{\partial \lambda_i} \right)_{\lambda_i = \lambda_i^k}$ in Green's MAP reconstruction algorithm (eqn.6) by $\frac{1}{\beta}\Delta_T^k(i')$, we get a new reconstruction algorithm, given by,

$$\lambda_{i'}^{k+1} = \frac{\lambda_{i'}^k}{\left[\sum_{j=1}^M p_{i'j} + \frac{1}{\beta}\Delta_T^k(i') \right]} \sum_{j=1}^M \frac{y_j p_{i'j}}{\sum_{o=1}^N \lambda_o^k p_{oj}} \tag{11}$$

where, coordinates (i,j) is denoted by a single coordinate $\{i' = (i-1) * \sqrt{N} + j\}$. In the iterative

image reconstruction procedure, the final correction term is fed back to update the pixel after each iteration. The iterations are continued until acceptable convergence is obtained.

Here, the uncertainty arises from the inability to correctly anticipate the pixel values (emission density) from the incomplete projection data obtained from the PET measurement system due to dimensional instability and the detector inefficiency.

In the proposed approach, the reconstruction process benefits from the consequence of the correct estimation of edges in the neighborhood. Suppose, using the current estimate, the system makes a decision that at a pixel location (i, j), an edge is present or an edge is absent. This decision leads to a lowering of percent error.

In PET, the goal seeking paradigm is defined as: Find a decision (presence/absent of edge), so that the outcome (reconstructed image) is acceptable within a predefined tolerance limit of the desired error metric.

4. Summary of the Proposed Algorithm

Table 1: Proposed Algorithm

Begin 1. Precompute the annihilation-detection probabilities $Q = [p_{ij}],\ i = 1, ..., N,\ j = 1, ..., M$ for all the pixels and the corresponding detector tubes. 2. Obtain the sensor (detector) reading $y_j;\ j = 1, ..., M$. 3. Assume the initial estimate to be uniformly distributed positive value $\lambda_i^0 = 0.01$. 4. Calculate the local derivatives for all the pixels along all the 8 directions and the final correction term $\Delta_T(i')$, where, $\{i' = (i-1) * \sqrt{N} + j\}$(eqn.10). 5. For $j = 1, ..., N$, calculate the pseudo-projections $\phi_j^k = \sum_{i=1}^{N} \lambda_i^k p_{ij}$ and the calculate the error $\psi_j = (y_j - (1 + \frac{1}{\beta}\Delta_T(i')\phi_j)$. 6. Now, calculate the feedback term, $\Delta(\lambda_{i'}^k) = \frac{\lambda_i^k}{\sum_{j=1}^{M} p_{ij} + \frac{1}{\beta}\Delta_T(i')} \sum_{j=1}^{M} \frac{\psi_j}{\phi_j} p_{ij}$. 7. Update the pixel values using, $\lambda_{i'}^{k+1} = \lambda_{i'}^k + \Delta(\lambda_{i'}^k)$. 8. Continue the iterations until acceptable convergence is obtained. End

Summary of the proposed algorithm is shown in Table.1.

5. A Case Study of goal seeking Paradigm

5.1. Simulated PET System

The algorithm has been tested on a simulated PET system. The PET system has been configured with 128 detectors, equivalent to 4160 detector tubes. The object space is decomposed into 128×128 square pixels. The object space is a square region inscribed within the circular detectors. An electron-positron annihilation event occurring inside a pixel is governed by a number of physical phenomena such as attenuation, scattering, absorption and detector characteristics. All these physical processes have a bearing on the probability matrix. In this study, we assume that the probability of an emission in box i and its detection in tube j depends only on the geometry of the measurement system. In such a case, an annihilation event in box i, getting detected in a tube j with the probability p_{ij} is proportional to the angle of view from the center of the box i in to the detector tube j, i.e, $p_{ij} = \frac{\theta_{ij}}{\pi}$. Shepp *et al.* [2] have shown that the choice of p_{ij} based only on the geometry of the measurement system is reasonable, and that the results of the reconstruction do not depend critically on the choice of p_{ij}. Before the reconstruction begins, the probability matrix $\mathbf{P} = [p_{ij}]$,$i = 1, ..., N$ and $j = 1, ..., M$ is precomputed and stored.

For simulating measurement data, a Monte Carlo procedure is used [3][24][25]. In Monte Carlo procedure, one uses random numbers to conduct experiments. Here, we are trying to learn a new system that involves some randomness, and we wish to learn what behavior can be expected without actually watching the real system. We first formulate a mathematical model by identifying the key random variables which describe the PET system. For generating the simulated measurement data, the following steps are followed:

(1) First, a random pixel is chosen in the test phantom (The concentration of the radionuclei at the given pixel is assumed to be proportional to the emission density of the pixel).

(2) This point is taken as the emission point with probability proportional to the density values of the pixel at that point. This makes sure that higher density points are chosen more often.

(3) For each of the accepted emission point, a randomly oriented line (between 0 to π radians) is selected and the pair of detectors with which this line intersects are found. The random line

corresponds to the direction in which the pair of annihilated photons travel.

(4) The detectors which this line intersect are assumed to detect this annihilation event and the count corresponding to this pair of detectors is incremented.

(5) Steps (1)-(4) are continued for every count which corresponds to an annihilation event. Normally, the number of counts are taken as large as 100,000.

(6) In this way, all the emissions are simulated and counted in the respective tubes. The array of tube counts is taken as the measurement data for image reconstruction.

We have used a source image with different density values and a total of 100,000 emission counts for the simulation studies.

5.2. Algorithm Evaluation and Comparison of Performance

All the evaluation tests defined in this section are carried out on a simulated PET system. In the present paper two different phantoms are used for algorithm evaluation. The proposed algorithm with a 5×5 neighborhood window is used. The results are also compared with those reconstructed using MAP reconstruction algorithm. MAP with potential $V(\lambda_i - \lambda_j) = \sum_{j \epsilon N_i} (\lambda_i = \lambda_j)^2$ and $\beta = 2.5 \times 10^4$ is used in the present study. This choice of β has produced the best estimate and hence this value of β is used for this study. In general, the algorithm is found to converge for the β values in the wide range $[10^3 - 10^7]$. The images were tested for both the proposed new algorithm and as well as the existing ML and MAP algorithm. The performance of the proposed algorithm is evaluated using 5 different metrics.

5.2.1. Visual Inspection

Figs. 4 (b), (c) and (d) show the reconstructed images using ML, MAP, median root prior (MRP) [19][20] and the proposed algorithm after 50 and 100 iterations respectively. For quality assessment, the original test image(phantom) is also shown (see Fig.4(a)). The images reconstructed using the proposed algorithm (see Fig.4 (d)) are more appealing and rich in edges. The proposed algorithm compares favorably with the MAP and MRP algorithms.

5.2.2. Residual Error

The residual error measures the deviation of the generated pseudo-projections ϕ_j^k of the recon-

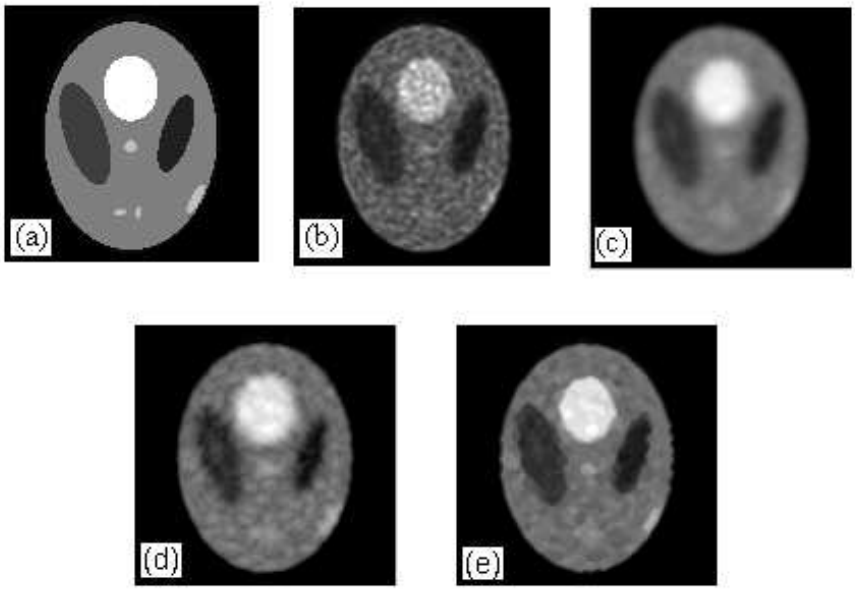

Figure 4: (a) Original phantom, (b), (c), (d) and (e) are the reconstructed images using ML, MAP, MRP and the proposed algorithm respectively.

structed image from the observed projection data y_j. Residual error $\rho(\lambda^k)$ at k^{th}-iteration is given by,

$$\rho(\lambda^k) = \sum_{j=1}^{M} (y_j - \phi_j^k)^2 \tag{12}$$

where, $\phi_j^k = \sum_{i=1}^{N} \lambda_i^k p_{ij}$ is the pseudo-projection in the tube j at k^{th} iteration. Fig. 5 shows the residual error of the reconstructed images using MAP, MRP and proposed algorithm. From these plots, it is clear that the proposed algorithm has the lowest residual error compared to the MAP and MRP algorithms. From these plots, it can be seen that the proposed algorithm requires fewer number of iterations for obtaining an image with desired low residual error compared to MAP and MRP algorithms.

5.2.3. Reconstruction with coarse and fine edge phantoms

To further substantiate the potential of the new approach, we have verified the performance of the proposed algorithm for phantom with coarse and fine edges. Both the phantoms are used to bring out the feasibility of the proposed algorithm. Figs. 6 and 7 show reconstructed images for coarse and fine edge phantoms. Figs. 6(b,c,d,e) and Fig. 7(b,c,d,e) are the reconstructed images after 50 iterations of ML, MAP, MRP and the proposed algorithm respectively. The MAP algorithm

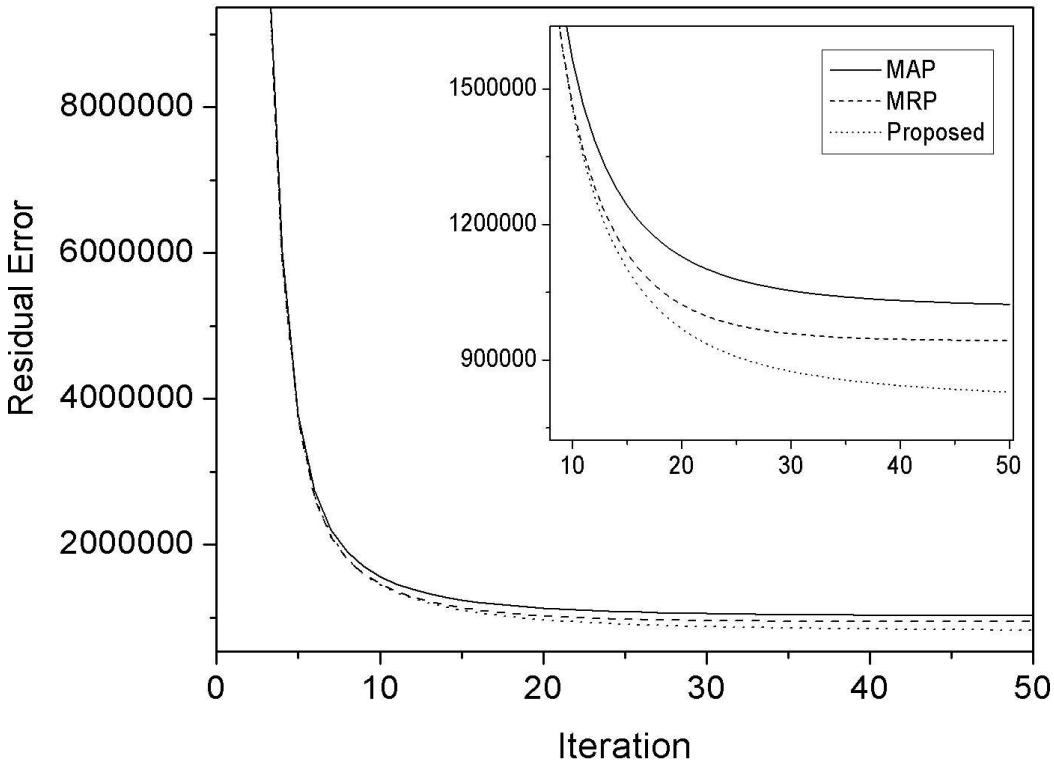

Figure 5: Residual error versus iteration plot for MAP, MRP and the proposed algorithm.

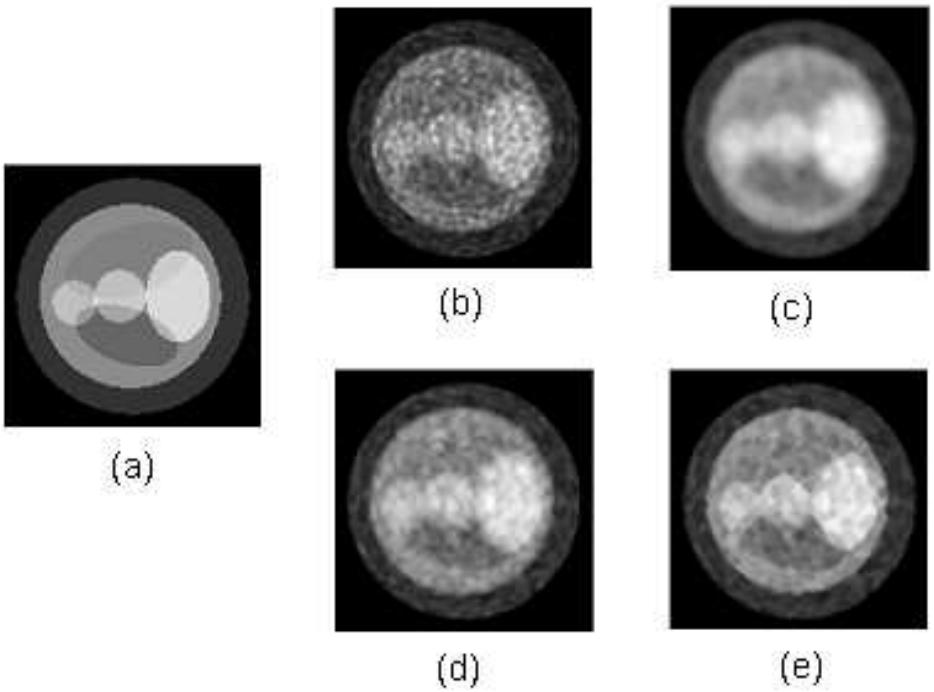

Figure 6: (a) Original phantom,(b),(c) and (d) are respectively the reconstructed images using MAP, MRP, and proposed algorithm for a coarser phantom.

has resulted in over-smoothened image, while MRP is found to produce streaking artifacts. The proposed algorithm has produced artifact-free reconstruction. Robustness for phantom with both coarse and sharp edges is evident from the reconstructed images.

5.2.4. Percent Error

For Qualitative measure of image quality, percent error is calculated after each iteration. This was proposed by S. J. Lee [22] as a measure of image quality. Percent error is defined by,

$$\xi^k = \frac{||\lambda^k - \tilde{\lambda}||}{||\lambda^k||} \times 100\% \tag{13}$$

where, λ^k is the k^{th}-reconstructed image, $\tilde{\lambda}$ is the true image and $||\bullet||$ is the L_2 norm. Fig. 8 shows that the proposed algorithm significantly improves the quality of reconstruction in terms of percent error. Percent Error for the proposed algorithm is found to be lower than those produced by ML, MAP and MRP algorithms. Dimensional Instability problem is reflected in the ML plot, similar to those obtained using χ^2-test obtained by Veclerov et al. [21].

5.2.5. Reconstruction with 3×3 and 5×5 window

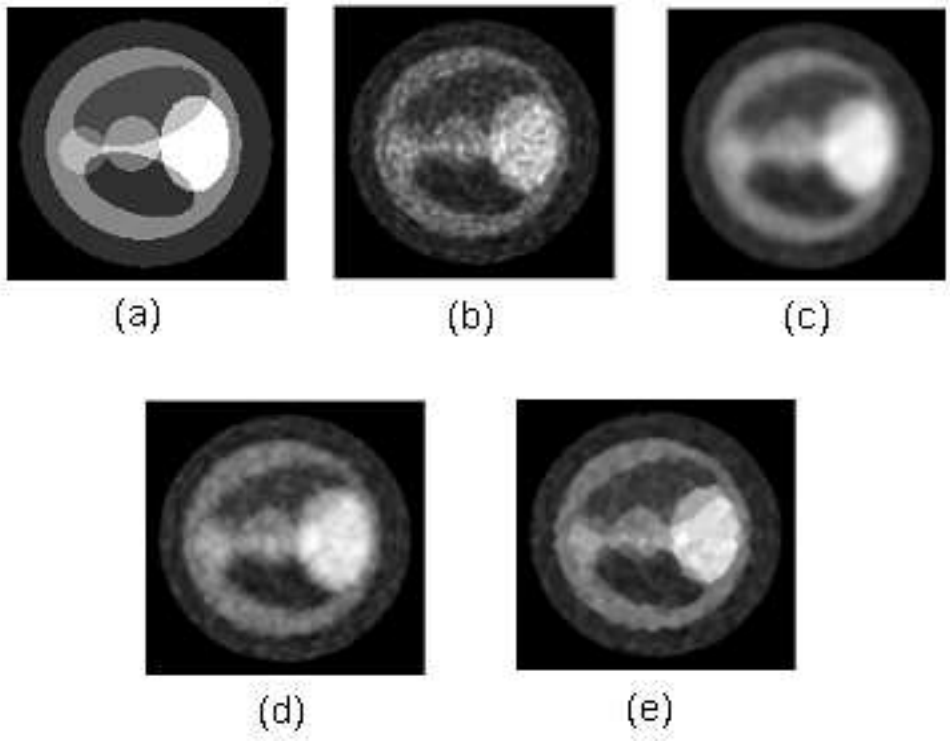

Figure 7: (a) Original phantom,(b),(c) and (d) are respectively the reconstructed images using MAP, MRP, and proposed algorithm for a sharper phantom.

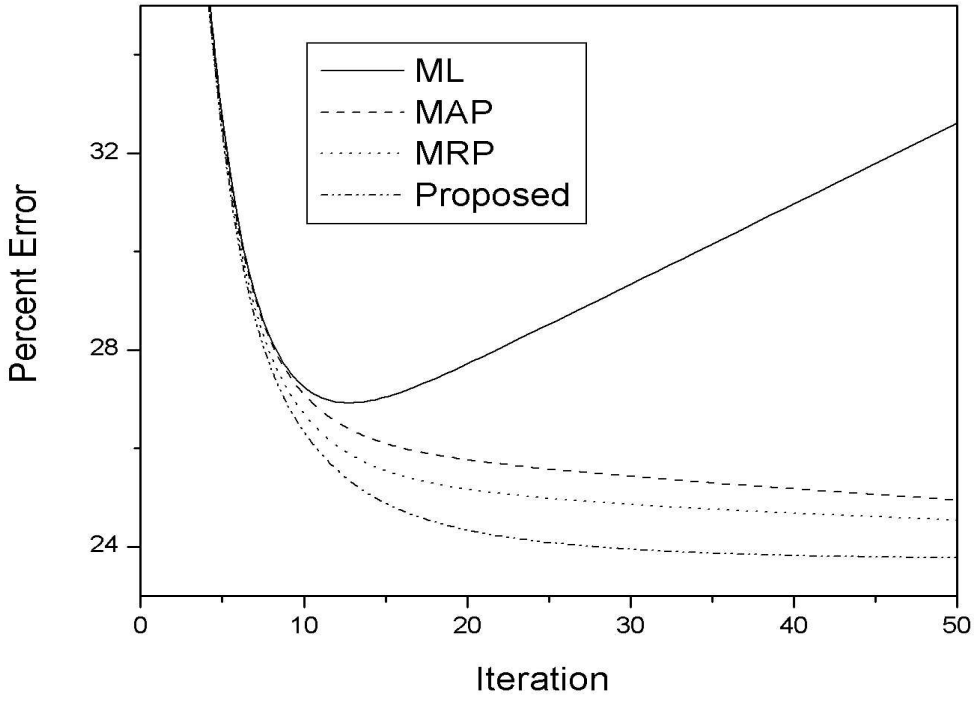

Figure 8: Percent error versus iteration plot for ML, MAP, MRP and the proposed algorithm.

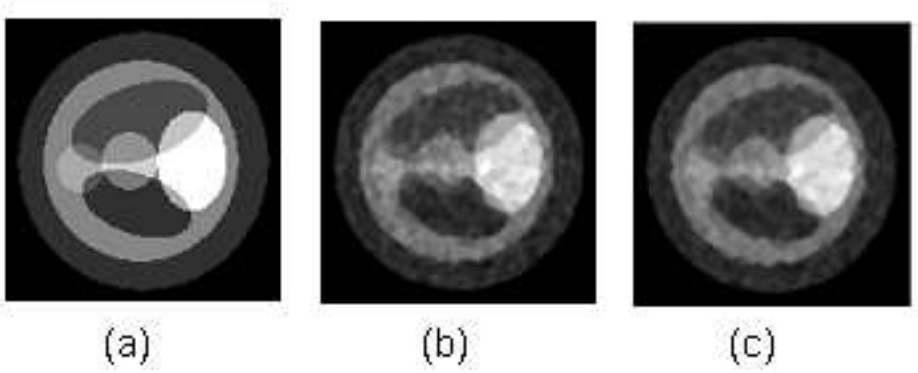

Figure 9: (a) Original phantom, (b) and (c) are the reconstructed images using the proposed algorithm with 3×3 and 5×5 window.

To understand the effect of interaction of a pixel with its neighborhood population on the reconstructed image, we have implemented the algorithm for two different neighborhood window sizes viz. 3×3 and 5×5. The proposed algorithm is found to produce smoother images with a 5×5 window compared to a 3×3 window. This could be because of the pronounced short range spatial correlation present in the reconstructed image. This is well evident form the reconstructed images shown in Figs. 9(b) and (c). The original test phantom (Fig. 9(a)) is also shown for comparison.

6. Conclusions

In this paper, we have presented a new goal seeking approach for PET image reconstruction. This is based on the integration of goal seeking approach with rule based techniques to model the potential function (which accounts for the nearest neighbor interaction) in an image reconstruction problem. A comparison of performance is discussed and the new approach promises a marked improvement in the quality of the reconstructed image compared to the those generated by existing ML, MAP and MRP algorithms.

Acknowledgement

The first author would like to thank Council of Scientific and Industrial research (CSIR), Government of India, for providing Junior Research fellowship. He declares that this work is partially supported by CSIR, New Delhi, India. The author Professor S. S. Iyengar was a visiting Satish

Dhawan Chair Professor at the Indian Institute of Science, Bangalore, India.

References

[1] M. E. Phelps, "Positron Emission Tomography provides molecular imaging of biological processes", Proc. Nat. Acad. Sci., vol. 97, No.16, pp.9226-9233, 2000.

[2] Y. Vardi, L. A. Shepp, and L. Kaufmann, "A statistical model for positron emission tomography ", J. Amer. Stat. Assoc., vol. 80 , pp. 8-37, 1985.

[3] L.A. Shepp and Y. Vardi., "Maximum likelihood estimation for emission tomography ", IEEE Trans. on Medical Imaging ., MI-1: pp. 113-121, 1982.

[4] Chen, C. M. and Lee, S. Y.: 'A parallel implementation of 3-D CT image reconstruction on hypercube multi processor', IEEE trans. Nucl. Sci., June 1990, vol.37(3), pp.1333-1346.

[5] K. Rajan, L. M. Patnaik and J. Ramakrishna, " High speed computation of the EM algorithm for PET image reconstruction ", IEEE trans. Nucl. Sci., Vol. 41, No.5, pp.0-5, Oct. 1994.

[6] Ranganath, M. V., Dhawan, A. P. and Mullani, N.: 'A multigrid expectation maximization algorithm for positron emission tomography', IEEE Trans. Med. Img., 1988, vol.7, pp. 273-278.

[7] Tanaka, E.: 'A fast reconstruction algorithm for stationary positron emission tomography based on a modifie EM algorithm', IEEE Trans. Med. Img., 1987 vol.3(1), pp.98-105.

[8] Lange, K., Bahn, M. and Little, R.: 'A theoretical Study of some maximum likelihood algorithm for emission and transmission tomography', IEEE Trans. on Med. Img., 1987, vol.6(2), pp. 106-114.

[9] Hudson, H. M. and Larkin, R. S.: 'Accelerated image reconstruction using ordered subsets of projection data', IEEE Trans. on Med. Img., 1994, vol.13(4), pp.601-609.

[10] Hudson, H. M., Hutton, B. F. and Larkin, R.: 'Accelerated EM reconstruction using ordered subsets', Jl. Nuc. Med., 1992, vol.33, pp. 960.

[11] Browne, J. and De Pierro, A.: 'A row-action alternative to the EM algorithm for maximizing likelihoods in emission tomography', IEEE Trans. on Med. Img., Oct. 1996, vol.15, pp. 687-699.

[12] Lalush, D. S., Frey, E. C. and Tsui, B. M. W.: 'Fast maximum entropy approximation in SPECT using RBI-MAP algorithm', IEEE Trans. on Med. Img., Apr. 2000, vol.19, pp. 286-294.

[13] T. Hebert and R. Leahy, " A generalized EM algorithm for 3-D Bayesian reconstruction from Poisson data using Gibbs priors ", IEEE Trans. on Med. Img., MI-8(2) : pp. 194-202, 1989.

[14] E. Levitan and G.T. Herman. " A maximum a posteriori probability expectation maximization algorithm for image reconstruction in emission tomography ", IEEE Trans. on Med. Img., MI-6(3) : pp. 185-192, 1987.

[15] P.J. Green, "Bayesian reconstruction from emission tomography data using a modified EM algorithm", IEEE Trans. on Med. Img., vol.9, No.1, March, 1990.

[16] Z. Zhou, R. M. Leahy and J. Qi, " Approximate maximum likelihood hyperparameter estimation for Gibbs prior ", IEEE Trans. on Img. proc., Vol.6, No.6, pp.844-861, June, 1997.

[17] J. Nuyts, D. Bequ, P. Dupont, and L. Mortelmans, "A Concave Prior Penalizing Relative Differences for Maximum-a-Posteriori Reconstruction in Emission Tomography ", IEEE Trans. on Nucl. Sci., Vol. 49, No. 1, pp.56-60, Feb. 2002.

[18] S. S. Iyengar, S. Sastry and N. Balakrishnan, "Foundations of data fusion for automation", IEEE Instrumentation and Measurement Mag., vol.6, No.4, pp.35-41, Dec. 2003.

[19] S. Alenius and U. Ruotsalainen, " Using Local Median as the Location of Prior Distribution in Iterative Emission Tomography Reconstruction ", IEEE Tran. Nucl. Sci., Vol.45, No.6, Dec. 1998.

[20] S. Alenius and U. Ruotsalainen, " Generalization of Median Root Prior Reconstruction ", IEEE Trans. Med. Img., Vol.21, No.11, Nov., 2002.

[21] E. Veclerov and J. Llacer , " Stopping rule for MLE algorithm based on statistical hypothesis testing ", IEEE Trans. on Med. Img., MI-6, pp. 313-319, 1987.

[22] S. J. Lee, "Accelerated Deterministic Annealing Algorithms for Transmission CT Reconstruction Using Ordered Subsets", IEEE Trans. Nucl. Sci., Vol.49, No.5, Oct. 2002.

[23] J. Besag , " Spatial interaction and the statistical analysis of lattice systems ", Jl. of Roy. Stat. Soc. B, Vol.36, pp. 192-236, 1974.

[24] N. Rajeevan, K. Rajgopal and G. Krishna. " Vector-extrapolated fast maximum likelihood estimation algorithms for emission tomography ", IEEE Trans. on Med. Img., Vol. 11, No.1, March 1992.

[25] L. Kaufmann, " Implementing and accelerating the EM-algorithm for positron emission tomography ",IEEE Trans. Med. Img., Vol. MI-6, pp.37-51, Mar. 1987.

[26] Snyder, D. L. and Miller, M. I.: 'The use of sieves to stabilize images produced with the EM-algorithm for emission tomography', IEEE Trans. Nucl. Sci., 1985, vol.32(5), pp. 3864-3872.